International Journal of Rotating Machinery
2000, Vol. 6, No. 4, pp. 253–263
Reprints available directly from the publisher
Photocopying permitted by license only

Influence of the Gap Size Between Side Walls and Ribs on the Heat Transfer in a Stationary and Rotating Straight Rib-roughened Duct

R. KIML*, S. MOCHIZUKI and A. MURATA

Department of Mechanical Systems Engineering, College of Engineering, Tokyo University of Agriculture & Technology, Koganei-shi, Tokyo 184, Japan

(Received 2 April 1998; In final form 15 October 1998)

The objective of this study is to investigate a heat transfer phenomenon in a straight rib-roughened duct which represents a cooling passage of a modern gas turbine blade. Experiments were performed for ribs mounted perpendicularly to the main flow direction on two opposite sides of the duct for the following cases: (1) with no gaps, (2) with gaps = 0.33h and (3) with gaps = 1h between the side walls and ribs (where h is the rib height). The heat transfer results revealed significant differences among these three cases, showing that the existence of gaps increases the heat transfer. Particularly, the local heat transfer on the wall between the consecutive ribs is higher in the near-side wall region than in the central region. To shed some light on this phenomenon, flow visualization was conducted using the particle tracer method. The flow visualization results revealed the effect of gaps on the three-dimensional flow structure between the ribs. It was concluded that this structure caused the heat transfer enhancement in the near-side wall region.

Keywords: Gas turbine, Internal cooling, Forced convection, Ribs, Flow visualization

INTRODUCTION

The efficiency of a gas turbine engine can be improved by increasing the turbine inlet gas temperature. To do this we have to provide a turbine blade with cooling techniques such as forced convection cooling, impingement cooling, film cooling and their combinations in order to maintain acceptable airfoil temperature and secure blade life. Forced convective cooling is utilized to remove the heat that has entered to the blade interior by supplying air from the compressor through cooling passages inside the blade. In the case of rotating blade, as shown in Fig. 1, the behavior of the cooling air and the heat transfer mechanisms in the coolant passage are very complex due to the interaction of (1) the

* Corresponding author. Tel.: 81 423 88 7088. Fax: 81 423 88 7088. E-mail: robert@mmlab.mech.tuat.ac.jp.

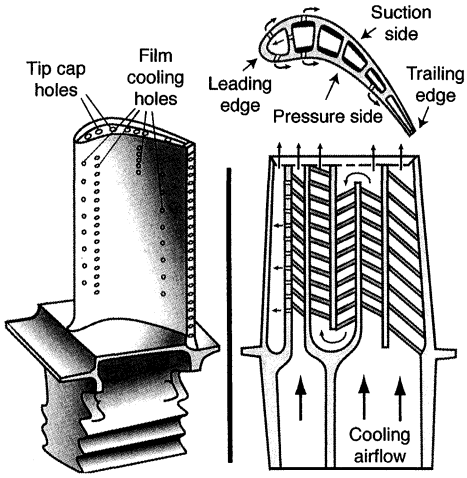

FIGURE 1 Schematic of internal and external cooling of a gas turbine rotor blade.

forced flow in the passage axis direction, (2) the secondary flow caused by the Coriolis force, (3) the buoyancy force caused by the centrifugal acceleration, (4) the secondary flow induced by the rib orientations and (5) the flow behavior between the consecutive ribs induced by gaps between the side walls and ribs.

The flow and heat transfer have been studied by many scientists. Taslim *et al.* (1991, 1994), Johnson *et al.* (1993, 1994), Mochizuki *et al.* (1997) and Duta and Han (1996) have mostly focused on the heat transfer in the entire passage. Those studies have provided us with the information about the heat transfer in an entire rib-roughened passage. However, with the advancement of gas turbine technology, it became necessary to know the detailed information of the local heat transfer distribution on the heat transfer surfaces in rib-roughened passages. For example, Rau *et al.* (1996) examined the Nusselt number enhancement and detailed velocity distribution between two ribs which were placed at 90° to the main flow direction. Ekkad and Han (1997) reported the detailed heat transfer distribution in two-pass square channels with rib turbulators placed at various angles to the main flow direction. El-Husayni *et al.* (1994) performed an experimental investigation to determine the effects of wall thermal boundary conditions on local heat transfer coefficient in stationary and orthogonally rotating turbulated square channels. All those studies, however, mainly reported flow and heat transfer measurements for the channels where there are no gaps between the side walls and ribs. Recently, experiments in a straight rib-roughened duct have been conducted by Balatka *et al.* (1997), they revealed the existence of strong three-dimensional flow structures between two successive ribs with gaps between the side walls and ribs.

In the present study, the effects of the gap size on the local heat transfer distribution between the consecutive ribs in a straight rib-roughened duct are examined. Flow visualization experiments are conducted for the stationary case and heat transfer experiments are performed for both stationary and rotating cases.

EXPERIMENTAL APPARATUS AND METHODS

Experimental Apparatus for Heat Transfer Experiment

The schematic of the test section installed on the rotor arm is shown in Fig. 2. Air from the ambient enters from the top and goes through a filter, honeycomb, wire gauze, contraction area to the test section. From the test section the air flows to a mixing screen and then turns 90° to a hollow shaft. Air temperature at the inlet to the test section is measured by means of four K-type thermocouples (0.3 mm in diameter). The mean bulk outlet temperature is measured by means of 17 thermocouples behind a flow mixing device which is installed at the exit of the test section.

The heat transfer experiment is performed in a straight rib roughened duct with a square cross section, 14×14 mm and duct length of 140 mm, as shown in Fig. 3. The ribs with a square cross section (rib height $h = 1.4$ mm) are mounted on the two opposite sides of the duct walls. The rib length to height ratio is 10. The test section is constructed

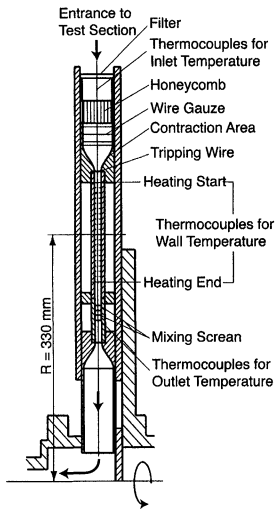

FIGURE 2 Schematic of rotor arm with the test section.

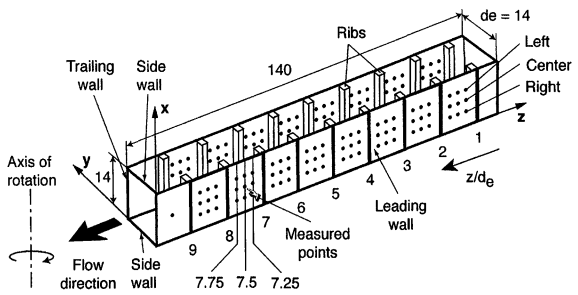

FIGURE 3 Detail of test section for heat transfer measurements with positions of rib-roughened and side walls in case of rotation.

from 5 mm thick Bakelite plates. This material is chosen for its low thermal conductivity, high mechanical strength and easy machining. The inside surfaces of the test section are covered with thin electric conductive plastic films which consist of 180 μm thick polyethylene terephthalate (PET) layer and a 20 μm thick conductive layer. Uniform wall heat flux conditions are achieved by passing an electric current through the conductive layer of the film which is originally used for high precision potentiometer. Its specific characteristics of highly uniform electric resistance fulfill the requirement for uniform heat generation. The test section and mixing device are insulated by an insulation material (SAN PERKA) with a heat conductivity of 0.0417 W/(mK). The insulation thickness is 20 mm.

The wall surface temperature is measured by means of 280 K-type thermocouples with a diameter of 50 μm. The thermocouples are located in three lines (Left, Center and Right) on the ribbed walls and in one line at the center of the side walls, as is presented in Fig. 3.

In the present study heat transfer measurements were carried out for ribs (1) with No Gaps, (2) with Small Gaps and (3) with Big Gaps between the side walls and ribs. The gap-size to rib-height ratio was (1) 0, (2) 0.33 and (3) 1, respectively. The Reynolds number (Re) was ranged from 10,000 to 20,000 which is almost in the same range as in a real situation. The Rotation number (Ro) was varied from 0 to 0.09 what is from several times to 10 times less than in a real gas turbine, therefore the influence of rotation will be much bigger under real turbine conditions.

To make a comparison among the walls of the duct they were given different names: Leading, Trailing and Side walls relative to the rotating direction, as is shown in Fig. 3. When the duct is rotated, the heat transfer in a straight rib-roughened duct changes due to the secondary flow caused by the Coriolis force. The Coriolis acceleration forces the central flow to hit the front wall in the rotating direction and so generates the secondary flow which creates a thinner hydrodynamic boundary layer at the front wall and a thicker boundary layer at the back wall, so that the heat transfer on the front wall (Leading wall) increases and on the back wall (Trailing wall) decreases.

The heat transfer on the two side walls in the case of rotation does not show any significant differences between them, therefore they were given the same name Side wall.

Experimental Apparatus for Flow Visualization Experiment

Flow visualization was carried out in a 6 m long water channel which was made of 10 mm thick transparent Plexi glass plates. The test section has a

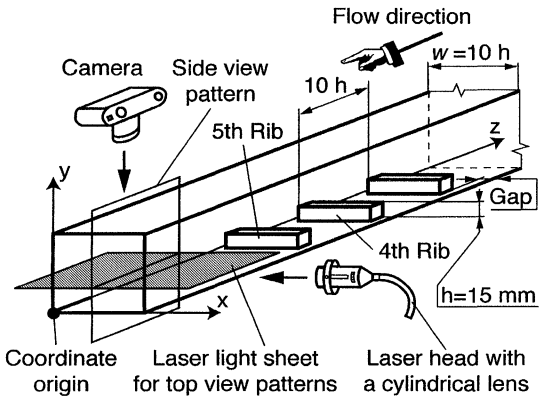

FIGURE 4 Schematic of flow visualization performed by particle tracer method.

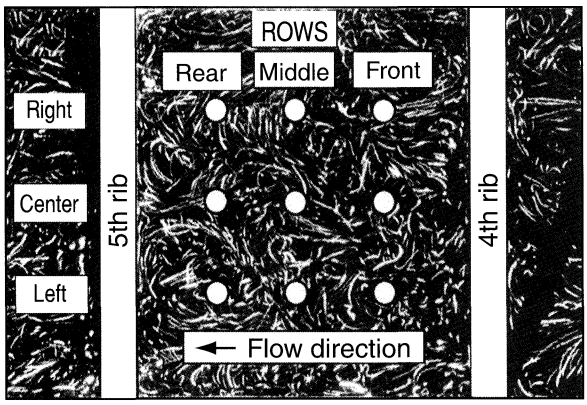

FIGURE 5 Positions of "Measured points" in which the heat transfer is measured.

square cross section (150 × 150 mm) with a free surface at the top of the channel and it was located 5 m downstream of the settling chamber. The water level was controlled and maintained at 75 mm from the bottom.

The ribs with a square cross section (15 × 15 mm) were made out of the transparent Plexi glass and mounted on the bottom of the channel perpendicularly to the main flow direction, as is shown in Fig. 4. Three types of ribs were used: (1) ribs with No Gaps, (2) ribs with Small Gaps and (3) ribs with Big Gaps between the adjacent walls and ribs. The gap-size to rib-height ratio was (1) 0, (2) 0.33 and (3) 1, respectively. Geometric proportions of the channel, ribs and gaps were the same as those used in corresponding heat transfer experiments. The Reynolds number (Re) was varied from 10,000 to 20,000.

The flow visualization was conducted using the particle tracer method (Balatka *et al.*, 1997; Nozicka, 1987), between the 4th and 5th ribs where the flow was fully developed. Water was mixed with the chemical compound $NaSO_4$ which increased the specific weight of the water so that the particles (70 μm in diameter) had the same specific weight as the water. They were illuminated by an argon laser light sheet (3 mm thick) and photographed by a still camera on a very sensitive (1600 ASA) film. The camera exposure time was set to 1 or 0.5 s to allow the particles to create path lines which were recorded on the film. Top view patterns were photographed at 4 locations $y = 0.33h$, $0.66h$, $1h$ and $1.33h$ from the bottom, as is depicted in Fig. 4. Side view patterns were obtained at $x = 5h$ (center), $2.66h$, $1.4h$ (only in the case with Big Gaps) and $0.66h$ (near-side wall region) from the side wall.

The corresponding positions for the heat transfer measurements are shown in Fig. 5. There are three rows of temperature measurement points: front, middle and rear. Each row has three measurement points (left, center and right) in spanwise direction.

Data Reduction

Nusselt, Reynolds, Rotation and Rayleigh numbers are defined, respectively, as follows:

$$Nu = \alpha d_e / k, \tag{1}$$

$$Re = u d_e / \nu, \tag{2}$$

$$Ro = \omega d_e / u, \tag{3}$$

$$Ra = R\omega^2 \beta \dot{q}_w d_e^4 Pr / (k\nu^2), \tag{4}$$

where α is the local heat transfer coefficient, d_e the equivalent diameter of the heat transfer duct or water flow visualization channel, k the thermal

conductivity of the air, u the mean velocity of the air (water), ν the kinematic viscosity of the air (water), ω the rotation angular velocity, β the volumetric expansion coefficient of the air and $\dot{q}_w$ the wall heat flux. All the physical properties k, ν, β and Pr are evaluated from the arithmetic mean temperature of the air at the inlet and exit of the test section.

An uncertainty analysis using the ASME Performance Test Code, 1986, was carried out during the heat transfer experiment and it estimated the maximum uncertainty in the Nusselt number to be less than 4% for the stationary case and less than 6% for the rotating case within the parameter range tested in the study.

RESULTS AND DISCUSSION

Influence of the Gap Size on the Flow Behavior Between Two Successive Ribs

Figure 6 shows the side and the top views of the flow between 4th and 5th ribs with No Gaps obtained by the particle tracer method. The side view patterns (Fig. 6(a) and (b)) show that the flow pattern near the side wall is very similar to that in the central region. It was observed that there is only small difference between the flow behaviors at those two locations. In both cases the fluid flows over the 4th rib, creates the frontal vortex behind the rib and produces the three-dimensional flow structure in the near bottom wall area, as can be seen in Fig. 6(c). The schematic of the flow structure, which was drawn on the basis of obtained results and visual observations, is illustrated in Fig. 7. In this figure the main three-dimensional character of the flow with approximate local flow directions is schematically shown.

Figure 8 indicates flow visualization results for the case with Small Gaps. The side view pattern taken in the near side wall region (see Fig. 8(a)) clearly shows the flow separation behind the 4th rib and flow reattachment taking place between the ribs at the bottom wall. Figure 8(b), which presents the flow in the vertical central plane of the channel,

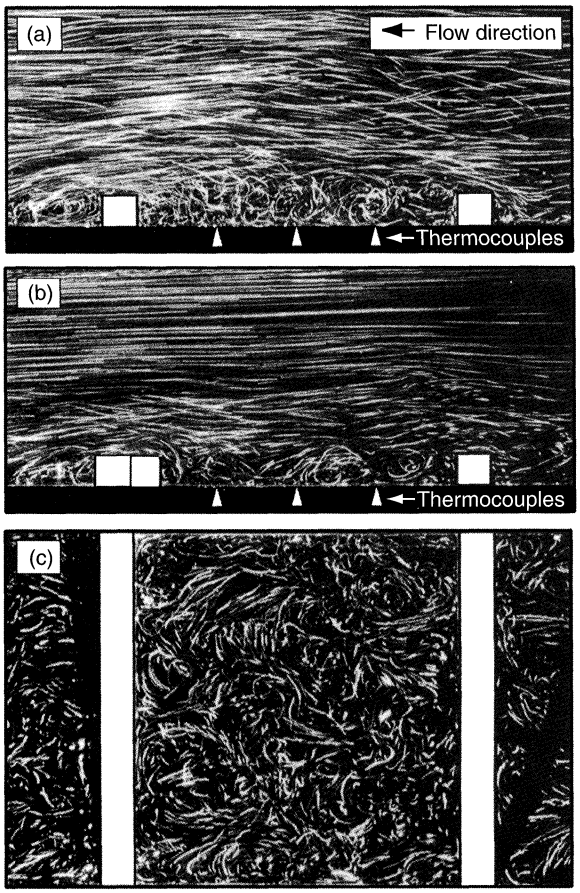

FIGURE 6 Flow around ribs with No Gaps, visualized by particles and laser light sheet, $Re = 10{,}000$. (a) Flow pattern at $x = 0.66h$ (near the side wall). (b) Flow pattern at $x = 5h$ (center). (c) Flow pattern at $y = 0.33h$ from the bottom.

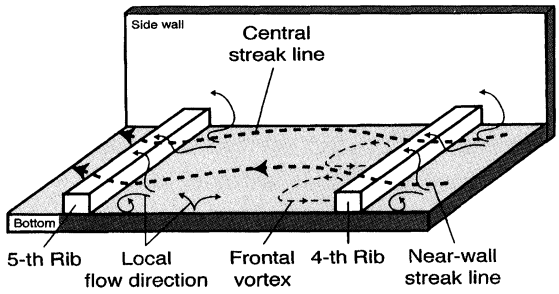

FIGURE 7 Schematic of flow pattern between 4th and 5th ribs with No Gaps.

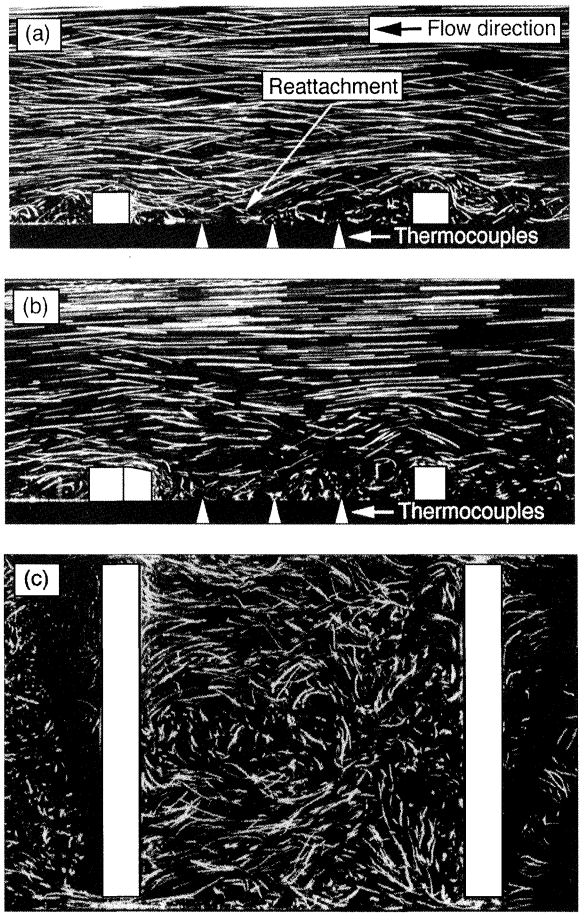

FIGURE 8 Flow around ribs with Small Gaps, visualized by particles and laser light sheet, $Re = 10{,}000$. (a) Flow pattern at $x = 0.66h$ (near the side wall), (b) Flow pattern at $x = 5h$ (center), (c) Flow pattern at $y = 0.33h$ from the bottom.

shows the separation area and that no flow reattachment is taking place at the center. The top view depicted in Fig. 8(c) shows the flow behavior at $y = 0.33h$ from the bottom surface of the water channel. Here the separation bubble immediately behind the 4th rib caused by the two vertical vortices shed from the gaps can be observed. Areas of flow reattachment can be found between the two ribs near the side walls. Through these figures it is confirmed that the flow structure behind the 4th rib is strongly three-dimensional and that it is more three-dimensional than in the case of No Gaps, as illustrated in Fig. 9.

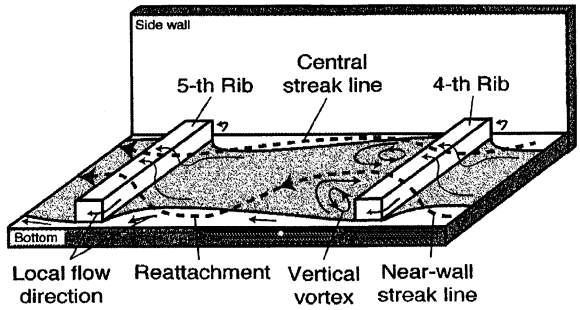

FIGURE 9 Schematic of flow pattern between 4th and 5th ribs with Small Gaps.

The flow visualization results for the rib with Big Gaps are presented in Fig. 10. The side view patterns were taken at three different locations ($x = 0.66h$, $1.4h$ and $5h$) to allow comparison with the two previous cases (No Gaps and Small Gaps). Figure 10(a) shows the side view obtained at $y = 0.66h$. It can be seen in this figure that the rib influence at this location is very small and the flow near the side wall is only slightly influenced by the flow which flows through the gap. The flow pattern taken at $1.4h$ from the side wall shows the situation $0.33h$ from the front rib edge, which is the same distance as in the case with Small Gaps (see Fig. 8(a)). Here it can be observed that the flow separation behind the rib and the flow reattachment between the ribs take place. The flow pattern at the central vertical plane (Fig. 10(c)) indicates the existence of a large separated flow region. In Fig. 10(a), (b) and (c), together with Fig. 10(d), one can clearly see the strong three dimensional flow structure formed by the flows shed from the gaps. The two vertical vortices behind the 4th rib force the flow in the center region to move upward. A schematic of this complicated flow behavior is illustrated in Fig. 11.

Influence of the Gap Size on the Heat Transfer under Stationary Conditions

Figure 12 shows the local Nusselt number distribution between the 7th and 8th ribs in stationary conditions for the three cases: (a) No Gaps,

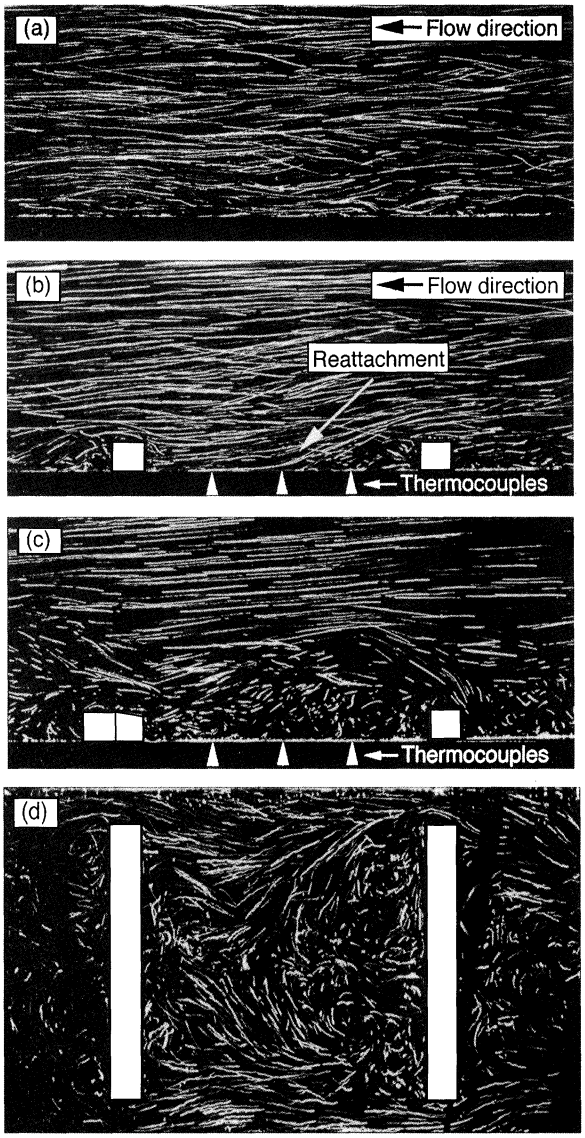

FIGURE 10 Flow around ribs with Big Gaps, visualized by particles and laser light sheet, $Re = 10{,}000$. (a) Flow pattern at $x = 0.66h$ (near the side wall). (b) Flow pattern at $x = 1.4h$ (near the side wall). (c) Flow pattern at $x = 5h$ (center). (d) Flow pattern at $y = 0.33h$ from the bottom.

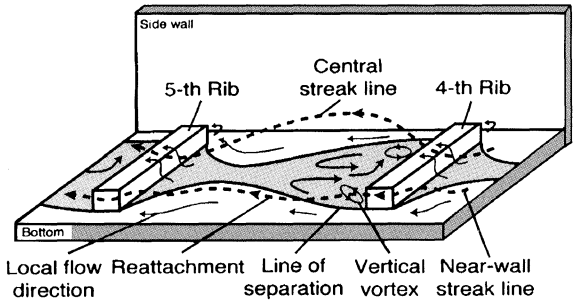

FIGURE 11 Schematic of flow pattern between 4th and 5th ribs with Big Gaps.

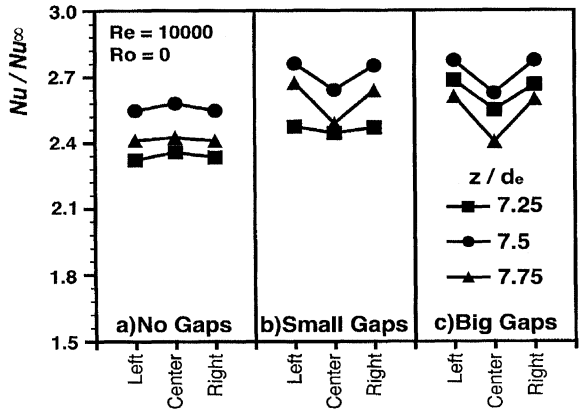

FIGURE 12 Local Nu distribution between 7th and 8th ribs in the stationary case.

(b) Small Gaps and (c) Big Gaps. In this figure, there are three rows of temperature measurement points, that is, front (■), middle (●) and rear (▲) which correspond to $z/d_e = 7.25$, 7.5 and 7.75, respectively. Each row has three measurement points (left, center and right) in spanwise direction, as is depicted Figs. 3 and 5.

In the case of No Gaps the Nusselt number at the front row (■) of the measurement points, just behind the 7th rib is relatively low. This is caused by the frontal vortex which covers the whole area of the front row (■), as illustrated in Fig. 7, therefore the Nu in this region is the lowest. Nu increases at the middle row (●) and deteriorates at the rear row (▲) due to the three-dimensional flow in the near bottom area, as shown in Fig. 6. It can be observed at those three rows of measurement points (■, ● and ▲) that Nu at the center is only slightly higher than those at the left and right. In contrast to the cases where the ribs are provided with gaps, the flow pattern in the central region is very similar to that in the near-side wall region and no significant

flow reattachment occurs in this case. The small differences in *Nu* among these three locations (right, center and left) are due to the spanwise uniformness of the flow.

In the case of Small Gaps, the Nusselt number is also the lowest at the front row (■) of the measurement points. It is the effect of the separation bubble behind the 7th rib which is produced by the two vertical vortices, as it was explained in Fig. 8(c). Contrary to common knowledge, *Nu* is significantly higher in the near-side wall region than in the central region at the middle (●) and rear (▲) rows. It is considered to be caused by (1) introduction of fresh air through the gaps to the region behind the rib, (2) the flow reattachment at the near-side wall region and (3) the separation area in the central region.

The gap effect on the heat transfer at all three rows (■, ● and ▲) of measurement points can be clearly observed especially in the case of Big Gaps. In contrast with the case of Small Gaps, spanwise distribution of *Nu* at the front row (■) is similar to that at the middle row (●) due to the presence of the strong three-dimensional vortices behind the 7th rib, as presented in Fig. 10(d) and 12. The Nusselt number at the rear row (▲) is lower than those at the middle row (●) and the front row (■). This is attributed to the boundary layer growth in the flow direction and its separation in front of the second rib.

The Nusselt number distribution along the central lines (center) of the rib-roughened and smooth Side walls in the stationary conditions for the three cases (No Gaps – NG, Small Gaps – SG and Big Gaps – BG) are shown in Fig. 13. It is shown in this figure that at first *Nu* decreases in the inlet region due to the thermal boundary layer growth, then it turns to increase because of the ribs, and up-and-down fluctuaction in *Nu* is repeated corresponding to the rib position. The difference of *Nu* distributions at the rib-roughened walls (●, ■ and ▲) and smooth Side walls (△, □ and ○) are clearly observed. Particularly, *Nu* at the smooth Side wall for the case of Big Gaps (○) is lower than that for the other two cases (Small Gaps (△) and

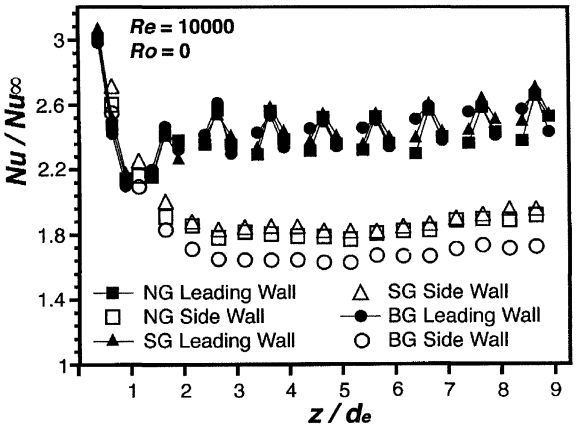

FIGURE 13 *Nu* distribution along the center lines of the Leading and Side walls for the stationary case.

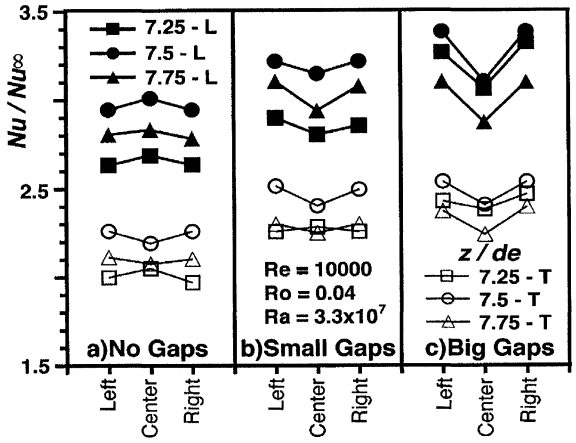

FIGURE 14 Local *Nu* distribution between 7th and 8th ribs in the rotating case.

No Gaps (□)). However, at the rib-roughened walls the Nusselt numbers in the cases with Big Gaps (●) and Small Gaps (▲) are higher than those in the case of No Gaps (■).

Influence of the Gap Size on the Heat Transfer under Rotating Conditions

The local Nusselt number distribution between the 7th and 8th ribs on the Leading wall (L) and Trailing wall (T) for the rotating case are shown in Fig. 14. It is obvious from the figure that the

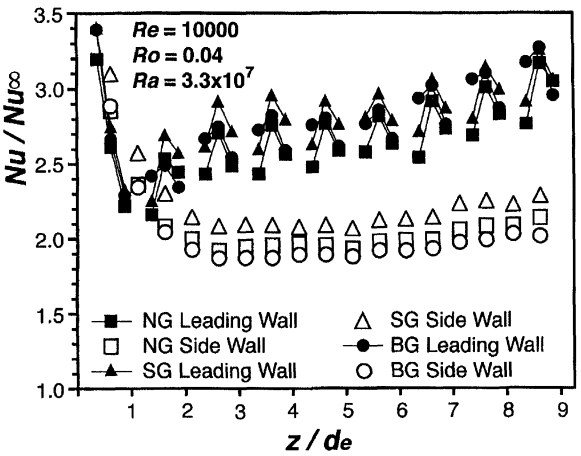

FIGURE 15 *Nu* distribution along the center lines of the Leading and Side walls for the rotating case.

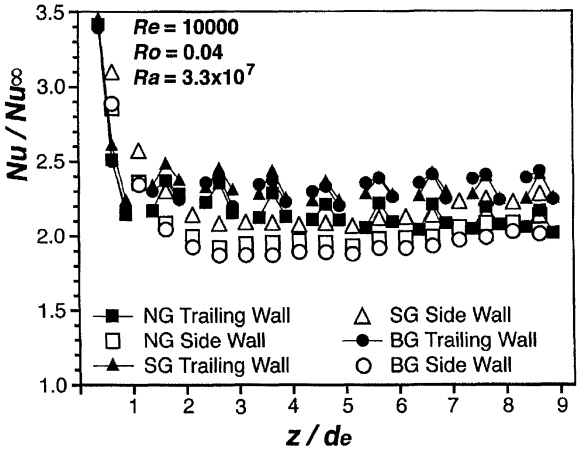

FIGURE 16 *Nu* distribution along the center lines of the Trailing and Side walls for the rotating case.

heat transfer on the Leading wall ((●), (■) and (▲)) is much higher than the heat transfer on the Trailing wall ((△), (○) and (□)) due to the secondary flow caused by Coriolis forces, as was explained previously. The effects of the gaps can be clearly observed by comparing the following three cases: (a) No Gaps, (b) Small Gaps and (c) Big Gaps.

Figure 15 presents the Nusselt number distribution along the central lines of the Leading and Side walls for three different gaps: No Gaps – NG, Small Gaps – SG and Big Gaps – BG. *Nu* at both Leading and Side walls decreases in the entrance region of the test section due to the boundary layer development. However, Nusselt numbers at the Leading wall ((▲), (●) and (■)) rebound at the location just after the first rib, and gradually increase with a development of the secondary flow caused by Coriolis forces. It can be seen in this figure that Nusselt numbers in the cases of Small Gaps (▲) and Big gaps (●) are higher than that of No Gaps (■). By comparing Figs. 13 and 15, one can see that rotation magnifies the effect of the gap size on the heat transfer.

The situation at the Trailing wall is completely different from that at the Leading wall, as is shown in Fig. 16. The Nusselt number in the case of No Gaps (■), after decreasing in the inlet region of the test section, slowly decreases due to the secondary flow caused by Coriolis forces and finally at the end of the test section *Nu* is equal or slightly less than that on the Side wall (□). When there are gaps (Small Gaps (▲) and Big Gaps (●)) the local heat transfer is affected by the gap effect so that the Nusselt number, in contrast with the case of No Gaps (■) is remaining approximately at the same level. It can be clearly observed in this figure that the gap effect becomes more obvious at the second half of the test section.

The Nusselt number at the smooth Side walls at first decreases in the inlet region due to the thermal boundary layer growth, then it slowly increases because of the secondary flow development. *Nu* is the highest in the case of Small Gaps (△) and significantly lower for the cases of Big Gap (○) and No gaps (□). By comparing Figs. 13 and 15, one can see that the rotation increases the heat transfer.

In Fig. 17, the comparison of the average *Nu* of the Ribbed and smooth Side walls is made for the stationary and rotating cases. At the Ribbed walls, average *Nu* increases with an increase of the gap size and it can be clearly observed especially for the case of rotation. At the Side wall the situation is more complicated. At first, the gap effect enhances *Nu* (NG → SG), but with a further increase of the gap size, *Nu* significantly decreases (SG → BG).

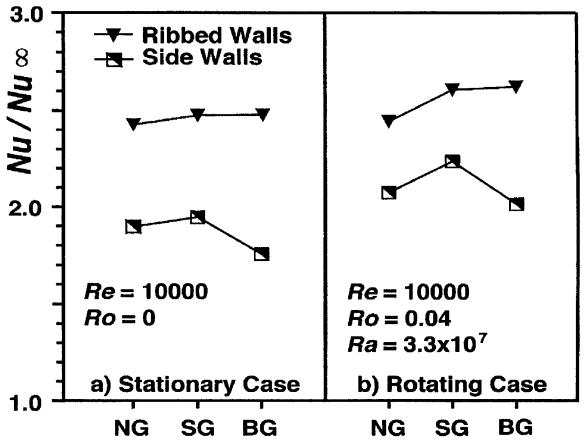

FIGURE 17 Average *Nu* distribution at the Ribbed and Side walls.

This phenomenon becomes more obvious in a rotating case when the flow is affected by the secondary flow due to Coriolis forces.

SUMMARY

The flow visualization and heat transfer experiments were performed for ribs mounted perpendicularly to the main flow direction. In order to examine the gap effects on the flow behavior and local Nusselt number distribution, three different rib arrangements were tested: (1) ribs with No Gaps, (2) ribs with Small Gaps and (3) ribs with Big Gaps between the side walls and the ribs.

The flow visualization results revealed strong three-dimensional flow structures due to the influence of the ribs, side walls and gaps. The existence of the gaps causes *Nu* enhancement in the near-side wall region of the rib-roughened walls due to (1) the introduction of the fresh air through the gaps to the region behind the rib, (2) the flow reattachment in the near-side wall region and (3) stronger three-dimensional flow than in the case of No Gaps.

The average Nusselt number at the Side walls increases with the existence of the gaps (Small Gaps), but with a further increase of the gap size, *Nu* significantly decreases (Big Gaps). This phenomenon becomes more obvious in the case of rotation when the flow is affected by the secondary flow due to Coriolis forces.

Acknowledgments

This work was partially supported by Grant-in-Aid for Scientific Research (No. 07455091) from the Ministry of Education, Science, Sport and Culture of Japan. The authors would like to express their gratitude to Dr. K. Balatka for his useful discussion and to Mr. T. Takahashi and Mr. S. Takeda who were very helpful in carrying out the experiments.

NOMENCLATURE

d_e	equivalent diameter
h	rib height
k	air thermal conductivity
u	air (water) mean velocity
z	duct length
$\dot{q}_w$	wall heat flux
w	channel width
R	average length of rotor arm
Re	Reynolds number
Ra	Rayleigh number
Ro	Rotation number
Nu	Nusselt number
Pr	Prandtl number
α	local heat transfer coefficient
ν	air (water) kinematic viscosity
β	air volumetric expansion coefficient
ω	angular velocity of rotation

References

Balatka, K., Mochizuki, S. and Murata, A. (1997) Visualisation of three dimensional flow around ribs in a duct, *The 1st Pacific Sym. on Flow Vis. and Image Proc., Proc. 1st Pacific Sym. on Flow Vis. and Image Proc.*, Honolulu, Vol. 1, pp. 219–224.

Duta, C., Han, J.-C. and Zhang, Y.-M. (1995) Influence of rotation on heat transfer from a two-pass channel with periodically placed turbulence and secondary flow promoters, *International Journal of Rotating Machinery*, **1**, 129–144.

Duta, C. and Han, J.-C. (1996) Local heat transfer in rotating smooth and ribbed two-pass square channels with three

channel oriantations, *ASME Journal of Heat Transfer*, **118**, 587–584.

Ekkad, S.V. and Han, J.-C. (1997) Detailed heat transfer distribution in two-pass square channels with rib turbulators, *International Journal of Heat Mass Transfer*, **40**(11), 2525–2537.

El-Husayni, Taslim, M.E. and Kercher, D.M. (1994) Experimental heat transfer investigation of stationary and orthogonally rotating asymmetric and symmetric heated smooth and turbulated channels, *ASME Journal of Turbomachinery*, **116**, 124–131.

Hu, Z. and Shen, J. (1996) Secondary flow and it's contribution to heat transfer enhancement in a blade cooling passage with discrete ribs, *Internationale Gas Turbine and Aeroengine Congress & Exhibition, Proc. Internationale Gas Turbine and Aeroengine Congress*, Birmingham, UK, June 10–13.

Johnson, B.V., Wagner, J.H., Steuber, G.D. and Yeh, F.C. (1993) Heat transfer in rotatting serpentine passages with selected model orientations for smooth or skewed trip walls, *ASME Paper* No. 93-GT-305.

Johnson, B.V., Wagner, J.H., Steuber, G.D. and Yeh, F.C. (1994) Heat transfer in rotatting serpentine passages with trips skewed to the flow, *ASME Journal of Turbomachinery*, **116**, 113–123.

Mochizuki, S., Murata, A. and Fukunaga, M. (1997) Effects of rib arrag. on pressure drop and heat trans. in a rib-roughened channel with a sharp 180° turn, *ASME Journal of Turbomachinery*, **119**, 610–616.

Rau, G. *et al.* (1996) The effect of periodic ribs on the local aerodynamic and heat transfer performance of a straight cooling passage, *International Gas Turbine and Aeroengine Congress & Exhibition Birmingham*, UK, June 10–13.

Nozicka, J. (1987) Aplication of experimental methods in fluid mechanics, *Proc. 10th FTM Congres Zilina*, Slovak Republic, **1**, 125–192.

Taslim, M.E. (1991) An experimental investigation of heat transfer coefficients in a spanwise rotating channel with two opposite rib-roughened walls, *ASME Journal of Turbomachinery*, **113**, 75–82.

Taslim, M.E., Li, T. and Kercher, D.M. (1994) Experimental heat transfer and friction in channels roughened witn angeled, V shaped and discrete ribs on two opposite walls, *ASME Paper* No. 94-GT-163.

MANEY
publishing

The Institute of Materials, Minerals & Mining

ENERGY MATERIALS

NEW FOR 2006

Materials Science & Engineering for Energy Systems

Maney Publishing on behalf of the Institute of Materials, Minerals and Mining

Economic and environmental factors are creating ever greater pressures for the efficient generation, transmission and use of energy. Materials developments are crucial to progress in all these areas: to innovation in design; to extending lifetime and maintenance intervals; and to successful operation in more demanding environments. Drawing together the broad community with interests in these areas, *Energy Materials* addresses materials needs in future energy generation, transmission, utilisation, conservation and storage. The journal covers thermal generation and gas turbines; renewable power (wind, wave, tidal, hydro, solar and geothermal); fuel cells (low and high temperature); materials issues relevant to biomass and biotechnology; nuclear power generation (fission and fusion); hydrogen generation and storage in the context of the 'hydrogen economy'; and the transmission and storage of the energy produced.

As well as publishing high-quality peer-reviewed research, *Energy Materials* promotes discussion of issues common to all sectors, through commissioned reviews and commentaries. The journal includes coverage of energy economics and policy, and broader social issues, since the political and legislative context influence research and investment decisions.

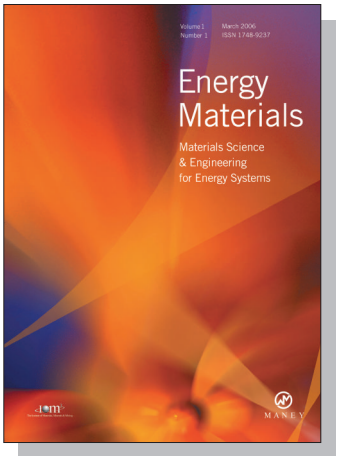

CALL FOR PAPERS

Contributions to the journal should be submitted online at **http://ema.edmgr.com**

To view the Notes for Contributors please visit: **www.maney.co.uk/journals/notes/ema**

Upon publication in 2006, this journal will be available via the Ingenta Connect journals service. To view free sample content online visit: **www.ingentaconnect.com/content/maney**

SUBSCRIPTION INFORMATION

Volume 1 (2006), 4 issues per year
Print ISSN: 1748-9237 Online ISSN: 1748-9245
Individual rate: £76.00/US$141.00
Institutional rate: £235.00/US$435.00
Online-only institutional rate: £199.00/US$367.00
For special IOM^3 member rates please email **subscriptions@maney.co.uk**

For further information please contact:
Maney Publishing UK
Tel: +44 (0)113 249 7481 Fax: +44 (0)113 248 6983 Email: subscriptions@maney.co.uk
or
Maney Publishing North America
Tel (toll free): 866 297 5154 Fax: 617 354 6875 Email: maney@maneyusa.com

For further information or to subscribe online please visit
www.maney.co.uk